Metrol. Meas. Syst., Vol. 32 (2025) No. 1, pp. 1–19
DOI: 10.24425/mms.2025.152774

PAN POLSKA AKADEMIA NAUK

METROLOGY AND MEASUREMENT SYSTEMS
Index 330930, ISSN 0860-8229
www.metrology.wat.edu.pl

M&MS

ANALYZING $BaSrTiO_3$ GAS SENSOR PROPERTIES UNDER NO_2 EXPOSURE: THE IMPACT OF IMPEDANCE SPECTROSCOPY

Bartłomiej Szafraniak[1)], Łukasz Fuśnik[1)], Jie Xu[2)], Feng Gao[2)], Andrzej Brudnik[1)], Sabina Drewniak[3)], Erwin Maciak[3)], Łukasz Błajszczak[4)], Artur Rydosz[1)]

1) Institute of Electronics, AGH University of Science and Technology, Al. Mickiewicza 30, 30-059 Kraków, Poland (✉ *szafrani@agh.edu.pl*)
2) State Key Laboratory of Solidification Processing, School of Materials Science and Engineering, Northwestern Polytechnical University, Xi'an 710072, China
3) Department of Optoelectronics, Silesian University of Technology, ul. Krzywoustego 2, 44-100 Gliwice, Poland
4) Department of Surface Engineering and Materials Characterization, AGH University of Science and Technology, Al. Mickiewicza 30, 30-059 Kraków, Poland

Abstract

Impedance spectroscopy is an appropriate technique for studying the complexity of materials, in which their different frequency relationships can be exploited in such a manner that they can be efficiently separated. Barium strontium titanate $BaSrTiO_3$ (BST) is a ferroelectric material with unique properties that make it useful in a range of electronic applications. BST plays an important role in the field of gas-sensing applications. The potential application of BST material as a gas sensor for detecting nitrogen dioxide (NO_2) in the atmosphere was studied. Impedance spectroscopy studies were conducted across a wide frequency range from 10^{-1} to 10^6 Hz, in the temperature range of 100°C to 350°C and a relative humidity of 50%, and both in air and the presence of NO_2 in concentrations from 0.5 to 5 ppm. The results of the impedance analysis indicate that the broadband models, which comprise both single and parallel RC elements, can accurately represent the NO_2 gas interaction mechanism with the gas-sensitive layer of the BST material. These models were found to effectively capture changes in parameters associated with the interaction.

Keywords: impedance spectroscopy, gas sensors, nitrogen dioxide, barium strontium titanate ($BaSrTiO_3$)

1. Introduction

Impedance spectroscopy (IS) is a technique used to study the electrical properties of materials over a range of frequencies [1]. The technique involves measuring the impedance of a material as a function of frequency, which can provide information about the electrical properties and structure of the material, including the study of solid-state materials [2, 3], biological systems [4–6], and electrochemical systems [7–9]. In solid-state materials, IS can be used to study the electronic and ionic transport properties as well as the dielectric properties of materials such as ceramics, polymers and semiconductors [6, 10]. The impedance spectroscopy method has been successfully applied to analyse *metal oxide* (MOX) semiconductor materials, *e.g.* gas sensors [11–15].

Article history: received March 11, 2024; revised September 12, 2024; accepted October 3, 2024; available online November 18, 2024.

In general, MOX-based gas sensors utilise the direct current DC mode of measurements; however, this has disadvantages in comparison with the use of alternating current (AC) [16]. One such example is the fact that the measurement of electrical properties using the DC method is greatly hampered by polarisation phenomena that occur in the measurement system. This causes an overestimation of the measured resistance value, and in the case of low-voltage measurements, it blocks the current flow [10]. The undoubted advantage of the AC method over DC measurements is that it provides information about the properties and processes occurring in the electrodes, on the surface of the material, in the inter-grain region and in the bulk [1, 16, 17]. This approach requires proper interpretation of the data but provides insight into the chemical and physical processes that influence the behaviour of semiconductor metal oxide gas sensors.

Nitrogen dioxide, a harmful air pollutant mainly from human activities such as vehicle and industrial emissions, can lead to health issues, notably for those with existing respiratory conditions. Linked by the WHO to respiratory infections, reduced lung function, and worsened asthma symptoms, high NO_2 levels can also heighten heart disease and stroke risks. Urban areas with heavy traffic often surpass WHO limits for NO_2, as seen in a 2018 EU study where over 80% of cities breached the 40 $\mu g/m^3$ guideline. Efforts to cut NO_2 include emission regulations, promoting alternative transportation, and using cleaner fuels such as natural gas [13, 18, 19].

Sensors used for the detection of NO_2 include electrochemical sensors [20], catalytic sensors, optical sensors based on infrared absorption (Infra-Red) and semiconductor ones, which are also referred to as resistance sensors. Moreover, sensors employ a variety of materials such as *molybdenum disulfide* (MoS_2) [21], *carbon nanotubes* (CNTs) [22] and graphene oxide [23]. However, it should be noted that the use of MOX-based NO_2 detectors is one of the most commonly studied approaches in the literature [24–26]. Numerous gas sensors are utilised for the detection of NO_2 [27].

Over the last few decades, gas sensors have been constantly developed with the utilisation of various gas-sensing materials, as discussed above. However, the 3S parameters of sensitivity, selectivity and stability remain the subject of research, and therefore novel materials such as *barium strontium titanate* (BST) draw the attention of the researchers. BST nanomaterials offer several advantages over their bulk counterparts, including a high dielectric constant, low dielectric losses, high piezoelectric coefficient, high Curie temperature and excellent optical properties [28, 29]. These unique properties make BST nanomaterials ideal for a wide range of applications, such as capacitors, sensors, energy harvesters, photodetectors, solar cells and optoelectronic devices [29–31]. Additionally, the ability to precisely control the size, shape, and composition of BST nanoparticles enables the optimization of their properties for specific applications, further expanding their potential uses [32, 33]. BST gas sensors have several advantages over traditional metal oxide gas sensors, including their high sensitivity and selectivity, low power consumption and rapid response time.

In addition to the applications mentioned above in which the properties of BST are typically exploited, BST plays an important role in the field of gas-sensing applications [28, 34, 35]. An example of the use of BST-based gas sensors to detect *nitrogen dioxide* (NO_2) is presented in the work of Patil *et al.* [36]. The authors tested the performance of BST layers with regard to the detection of various gases at different operating temperatures; a strong reaction was observed, inter alia, for *nitrogen dioxide* (NO_2) at room temperature. In addition, the work investigated the detection of gases at room temperature in terms of Sr doping concentrations in $BaTiO_3$ nanostructures. A different approach was presented by Stanoiu *et al.* [34]. The researchers of this work showed that the electrical resistance of $BaSrTiO_3$ material doped with 5% Cu increases during exposure to NO_2 at 3 ppm. Recently, we presented the preliminary results of a BST-based gas-sensing material that enables the detection of NO_2 [28]. Recent studies have shown that BST gas sensors can detect NO_2 concentrations as low as a few *parts per billion* (ppb) at room temperature, making them

Metrol. Meas. Syst., Vol. 32 (2025), No. 1, pp. 1–19
DOI: 10.24425/mms.2025.152774

useful for detecting NO_2 pollution in the atmosphere [28]. The sensing mechanism of BST gas sensors is based on changes in the electrical properties of the material, such as its capacitance, resistance and impedance, in response to NO_2 exposure. The performance of BST gas sensors can be improved by optimising the material properties and the design of the device, such as by modifying the grain size and crystal orientation of the BST thin films or by incorporating dopants into the material [34]. Additionally, the use of nanomaterials and composites can further enhance the sensing properties of BST gas sensors. BST gas sensors have potential applications in a range of fields, including environmental monitoring, industrial safety and medical diagnosis [36, 37].

This work focuses on the studies of gas-sensing responses of BST nanomaterials in the air as a reference and under NO_2 exposure from 0.5 to 5 ppm within a temperature range of 100°C to 350°C in *relative humidity* (RH) 50%. The aim is to find an electrically equivalent circuit model in the wide frequency range of 10^{-1} to 10^{6} Hz (and changes in its parameters) using an impedance spectroscopy measurement.

2. Materials and Methods

2.1. Gas-Sensor Substrates

A commercially available CC2 (conductometric electrode on corundum ceramic base pure platinum) electrochemical sensor for conductometric measurement with electrodes was used as a gas sensor substrate (Fig. 1) [13].

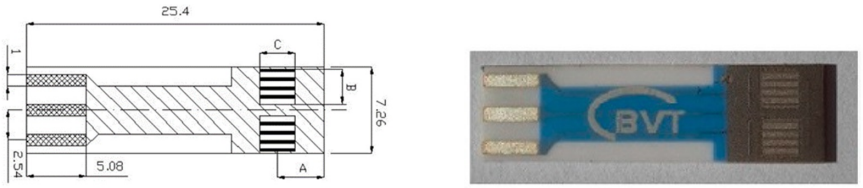

(a) (b)

Fig. 1. (a) scheme: dimensions A = 4 mm; B = 3 mm; C = 3 mm [38] (b) picture of the CC2 BVT gas-sensor substrate with deposited gas-sensing films.

Following the ultrasonic cleaning process, the gas-sensor substrates were transferred to the deposition chamber, in which the gas-sensitive layers were applied. Thin films of BST were deposited via magnetron sputtering onto the CC2 electrochemical sensor. In the catalogue note for our BVT CC2 electrochemical sensor, the active layer area is given by the formula $2 \times B \times C$, resulting in a value of 18 mm^2. The measured capacitance of the active area is determined to be 7.4 pF. The thickness of the deposited layer is 200 nm.

2.2. Gas-Sensitive-Layer Deposition

The gas-sensing layers were deposited using magnetron sputtering technology, during which a ceramic BST target was used. The industrial perspective drove the decision to apply magnetron sputtering technology to develop an effective and scalable deposition technology that can be easily applied in industrial applications that pave the way for large-scale fabrication of the sensors in the future for automotive applications. Moreover, thanks to the magnetron sputtering the front-end

electronics parts can be deposited by the same methods if other substrates (*e.g.* silicon) will be considered in future applications. RF currents (13.56 MHz) were used to sputter the BST ceramic disc. To increase the rate of the material deposition, magnetron sputtering technology was used, where a magnetic trap near the surface of the sputtered disc increases the degree of ionization of the working gas, causing an increase in the sputtering speed (yield). The BST powder used for the target fabrication was synthesized through the traditional solid phase method. The particle size reached around 0.11 μm after 24 h of ball milling. The BST target was prepared using a gel injection moulding process. Firstly, BST suspensions with solid loadings of 30–54 vol% were prepared by mixing the BST powder, 0.1–0.4wt% Isobam (based on the mass of the BST powder), and water in polyethylene containers for 24 h. Zirconia balls with diameters of 5–10 mm were used as the grinding media. The mass ratio between grinding media and BST powder is 1:2. The ball-milled material and the desired suspensions were cast into a plastic mould and gelled at 25–65°C for 5 h. The green bodies were de-moulded and put into an 80°C oven to dry for 24 h. Finally, the samples were sintered at 1400–1500°C for 3 h with a heating rate of 3°C/min and the BST target was subsequently obtained. The deposition system for co-sputtering has been previously presented [39]. The material characteristics have also been previously reported [28, 40–42]. A reactive sputtering method was used for the application of argon and oxygen at a ratio of 80% Ar/20% O_2.. The sputtering parameters were $5 \cdot 10^{-6}$ mbar, $2 \cdot 10^{-2}$ mbar, 205°C and 50W for the base vacuum, working pressure, deposition temperature, and power deposition, respectively. Due to the ceramic BST target being used, the RF (13.56 MHz) power supply (Huetinger, Germany) was set with 5W/min for increasing and decreasing the power ramp in pre-deposition and post-deposition processes. To enhance the gas-sensing properties such as long-term stability, the sensors were annealed at 400°C in the air for 4 h after deposition.

2.3. Gas-Sensing Measurements

A laboratory setup was utilised to measure the resistance of the sensor signal under changing conditions of humidity, gas concentration and temperature, as shown in Fig. 2. The measurement chamber had a volume of around 30 cm^3 and was heated by a resistive heater powered by an Agilent 6643A power source. The chamber contained the sensitive layers being investigated as well as a Pt100 temperature probe, which was linked to an Agilent 34970A digital multimeter. Humidity was measured immediately before the gas was added using a Sensirion SHT75 digital sensor manufactured by Sensirion AG in Zurich, Switzerland. Because the resistance of the sensor being studied varied significantly, a Keithley 6517 electrometer functioning in the constant voltage mode was employed. All equipment was controlled using a LabVIEW custom application, which was connected to a GPIB bus via an Agilent Technologies 82357B USB/GPIB interface card.

Bottles of air and NO_2 gas under investigation were supplied by the Air Products company and passed through mass flow valves/meters (model 1179 and 1459C, MKS Instruments, Deutschland, GmbH) in order to maintain a continuous gas flow. The set humidity level was obtained by controlling the flow of dry air passing through a bubbler with distilled water. The humidity level was kept at 1.8% throughout the stabilised conditions. The required concentration of NO_2 gas was achieved by controlling the ratio of the gas-to-air flow.

The concentration of *nitrogen dioxide* (NO_2) in the gas phase is affected by temperature due to the expansion and contraction of gases. According to the ideal gas law, when temperature increases, the gas expands, potentially reducing the concentration of NO_2 unless the gas volume is controlled. Conversely, lowering the temperature compresses the gas, increasing the NO_2 concentration in the same volume. This is especially important in systems without constant volume conditions [43]. The interaction of NO_2 with sensor materials (*e.g.*, metal oxides) is

Metrol. Meas. Syst., Vol. 32 (2025), No. 1, pp. 1–19
DOI: 10.24425/mms.2025.152774

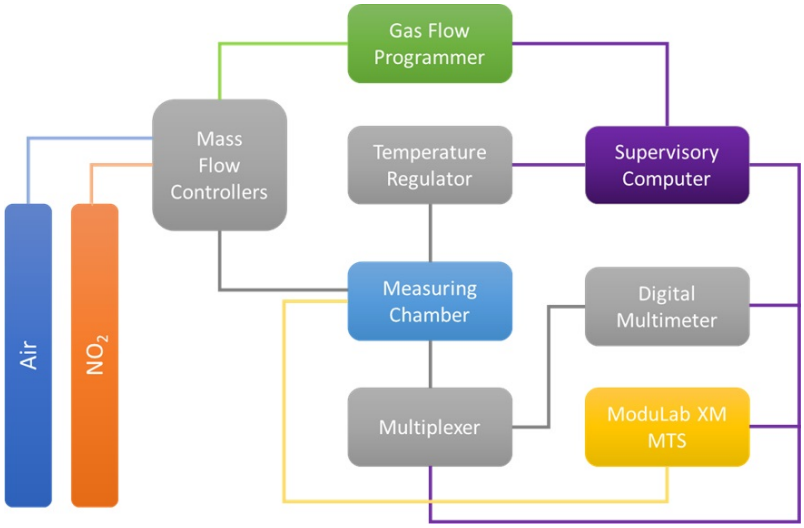

Fig. 2. Schematic diagram of a gas-sensing experimental setup for both AC and DC measurements.

highly temperature-dependent. At higher temperatures, NO_2 desorbs from the sensor surface, reducing its measurable concentration, whereas at lower temperatures, NO_2 tends to adsorb more, increasing sensor response. This phenomenon can introduce variability in the stability of NO_2 readings across a range of temperatures [44]. As it comes to sensor material properties most NO_2 sensors have materials whose electrical properties change with temperature. For example, metal oxide semiconductors have temperature-sensitive resistance and impedance, which affects their baseline behaviour and response to gas interactions. Temperature fluctuations can lead to signal drift, impacting the accuracy of NO_2 concentration measurements [45, 46]. High humidity levels can interfere with NO_2 sensor performance. Water molecules in the air can occupy active sites on the sensor surface, reducing the sensor's ability to adsorb NO_2, and thus leading to an apparent drop in measured NO_2 concentration. Additionally, water vapor can alter the dielectric properties of the sensor material, affecting its impedance and resistance characteristics [47]. In high-humidity conditions, NO_2 can react with water vapor to form nitrous acid (HONO) or nitric acid (HNO_3), reducing the available concentration of NO_2 in the air. This can lead to measurement instability as the NO_2 chemically transforms into other compounds. In a dynamic environment where humidity fluctuates, these reactions can result in significant changes in the detected NO_2 concentration [48]. Sensors, especially those based on metal oxides, can exhibit changes in impedance when exposed to high humidity. Water molecules can create a conductive layer on the sensor surface, altering its electrical characteristics and skewing the sensor's response to NO_2. This effect is more pronounced in materials with high surface porosity [49]. If the temperature drops below the dew point, condensation can form on the sensor surface or inside the gas flow system. This can create a physical barrier that prevents NO_2 from interacting with the sensor surface, causing a temporary loss of sensitivity. Condensation can also cause short-circuiting or unpredictable shifts in the electrical properties of the sensor, leading to erroneous readings [50]. When condensation occurs, water vapor condenses out of the gas stream, which effectively dilutes the gas phase concentration of NO_2. Since the total volume of gas is reduced, the concentration of NO_2 may appear to drop, even though the number of NO_2 molecules remains the same. This dilution effect becomes significant in high-humidity environments or when temperature fluctuations are abrupt [51]. As regards corrosion and sensor degradation, prolonged exposure to moisture from condensation can cause corrosion or

degradation of sensor materials. Metal-based sensors, in particular, are prone to corrosion under humid or wet conditions, leading to long-term drift and instability in NO_2 measurements. These effects are often irreversible, requiring recalibration or sensor replacement [52].

One of the fundamental parameters that characterise gas sensors is their response to the gas they are designed to detect. The sensor response (S) is defined by the formula:

$$S = \frac{R_0}{R_g}, \tag{1}$$

where:

R_0 – sensor resistance without the presence of gas,

R_g – sensor resistance in the presence of gas.

The DC measurement was performed in the temperature range of 25°C to 400°C, at a relative humidity (RH) of 50% (RH 50% was stabilized at 25°C). The total gas flow through the chamber was 500 sccm. The concentration of NO_2 applied was from 0.5 to 5 ppm. The temperature was rapidly changed every five measuring cycles of air (15 min) and air with various NO_2 concentrations (15 min). Both samples responded best to the presence of NO_2 at operating temperature. To determine the parameters of BST nanocomposites, a configuration based on an MTS Solartron ModuLab XM system was prepared. This enabled the determination of the impedance characteristics across a wide frequency range of 10^{-1} Hz to 10^6 Hz. Impedance spectroscopy measurements were conducted at different temperatures from 100°C up to 350°C in both air as a reference atmosphere and upon the introduction of NO_2 in relative humidity RH = 50%. The AC signal amplitude was set to 1 V. During the NO_2 exposure, the record of impedance spectra was analysed using ZView software [53].

In addition, the following factors have an impact on the resistance and impedance measurement method and the influence of the experimental system components and gas samples on the obtained results:

- Method of Measuring Resistance and Impedance:
  Combines the AC method with complex data analysis. The real and imaginary components of impedance are measured over a wide frequency range. The measured impedance data are fitted to an equivalent circuit model to interpret the physical processes within the material. Widely used in electrochemistry, materials science, and biological systems.
- Influence of Experimental System Components and Gas Samples:
  The type, material, and surface condition of electrodes can significantly influence the measurements. Poor contact or corrosion can introduce errors.
  Wiring and Connectors: Resistance in wires and connectors can add to the measured resistance or impedance, leading to inaccuracies.
  Temperature Control: Temperature fluctuations can affect the resistance and impedance of materials, as most materials have temperature-dependent properties.
  Gas Samples: Different gases can interact with the material being tested, altering its resistance or impedance. For example, certain gases might adsorb onto the surface of a sensor material, changing its electrical properties.
  The presence of moisture in the gas can significantly affect measurements, especially for materials sensitive to water vapor. Changes in gas pressure can alter the density and mobility of ions or electrons within the material, impacting the impedance.
- Practical Considerations:
  Regular calibration with known standards is crucial to ensure accuracy. Calibration compensates for systematic errors in the measurement setup. Proper shielding and grounding are essential to minimize noise and interference, particularly in AC measurements and

Metrol. Meas. Syst., Vol. 32 (2025), No. 1, pp. 1–19
DOI: 10.24425/mms.2025.152774

impedance spectroscopy. Consistent and careful sample preparation ensures reproducibility. Inhomogeneities or surface contaminants can lead to erroneous results. Maintaining a stable environment (temperature, humidity, and gas composition) during measurements helps in obtaining reliable data. Advanced data analysis techniques, such as fitting to equivalent circuit models, are necessary to interpret impedance spectroscopy data accurately. This requires expertise in both the theoretical and practical aspects of the system being studied.

By understanding and controlling these factors, more accurate and reliable measurements of resistance and impedance can be achieved, leading to better insights into the material or system under investigation.

3. Results

3.1. Characterisation of BST thin films

Scanning electron microscopy (SEM) and *energy dispersive X-ray spectroscopy* (EDS) images were obtained using an INSPECT S50 (FEI, Hillsboro, OR, USA) system. The SEM measurements were performed using an *Everhart-Thornley detector* (ETD) and the parameters were: HV- 20 kV, spot 5.0. Information about the elements (EDS spectroscopy) was collected using an Octane Elect Plus detector. The SEM measurements show that the BST material formed agglomerates with the size of 5 μm and smaller. The EDS measurements enabled the detection of the following elements: oxygen, aluminium, silicon, sulphur, titanium, strontium, barium, platinum and gold. Oxygen, silicon, strontium and gold were detected mainly in the area of agglomerates; however, it should be noted that gold is detected only in the area of smaller agglomerates. Barium, sulphur and titanium are detected in all areas and aluminium and platinum were detected mainly in the area between agglomerates. Moreover, it should be mentioned that the quantities of silicon, barium, titanium and sulphur are small. The Raman spectroscopy measurements were performed using an NTEGRA Spectra system (NT-MTD, Eindhoven, the Netherlands). Each spectrum was repeated five times in each area. The time of each measurement was 10 s, and the wavelength of the laser beam was 633 nm. Characterising the BST sensing layer using Raman spectroscopy offers several valuable insights. Raman spectroscopy is a non-destructive technique that provides information about molecular vibrations and the structural properties of gas receptors. When applied to the BST sensing layer, it can reveal detailed information about its chemical composition and potential changes in the layer's structure due to the thin film technology process or interactions with target analytes. The typical structure of bulk BST material is characterised by a rather complex Raman spectrum. The Raman spectra of BST consist of a broad peak centred at 235 cm^{-1}, a weak shoulder peak at 305 cm^{-1}, an asymmetric peak near 519 cm^{-1}, and a broad weak peak at 720 cm^{-1}. The peaks can be assigned to A1 (2TO), E (3TO + 2LO) + B1, A1 (3TO), and E (4LO) phonon modes, respectively [54]. For the purpose of analysing our receptors, we fabricated thin BST layers on two substrates. In addition to the proper *interdigital electrode* (IDT) CC2 substrate, the thin film structure was deposited on a glass substrate using the same technological process. These structures were then subjected to Raman spectroscopy analysis. Figure 3 illustrates a compilation of Raman spectra obtained for the BST layer on the CC2 substrate at three locations – on two electrodes, between the electrodes, and at two locations on the glass substrate. Raman spectra of BST samples are shown in Fig. 3.

Analysis of the broadband Raman spectrum of BST layers leads to the following conclusions: a weak Raman signal indicates strong amorphicity of the layers, which is also confirmed by our SEM/EDS studies. This is especially supported by the analysis of BST layers deposited on glass. Measurements conducted on the CC2 substrate electrodes revealed slightly more details due to the

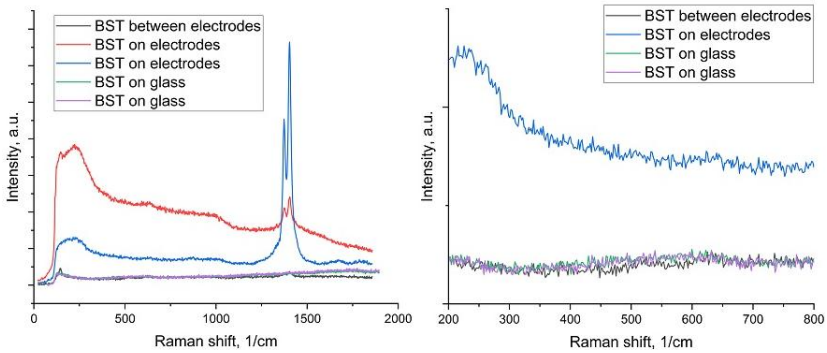

Fig. 3. Compilation of Raman spectra of BST structures on various substrates and at different locations within the structures: a) broadband, b) in the spectral range of 200-800 cm^{-1}.

Surface-Enhanced Raman Scattering (SERS) effect from the Pt/Au electrode material. The Raman signal above 800 cm^{-1} could not simply be attributed to the Raman vibration peak of BST films and may have actually been the fluorescence spectrum generated by electronic transitions [55]. Based on the literature, the peaks at 1370 cm^{-1} and 1400 cm^{-1} were attributed to the fluorescence spectrum produced by Cr^{3+} in Al_2O_3 [56]. Analysing the spectrum of the BST layers, the Raman spectroscopy indicates that the films do not exhibit a tetragonal structure. This is attributed to the absence of Raman active modes at 305 cm^{-1} and 720 cm^{-1} at room temperature. The Raman spectra of the films grown on CC2 and glass substrates consist of only one of the mentioned peaks – a broad peak at 235 cm^{-1}. However, their positions are slightly shifted compared to the bulk target material.

In Fig. 4 (zoomed red plot from Fig. 3), there can be seen one more band in the 520–700 cm^{-1} spectral range. The 634 cm^{-1} band is recognised as one of the disorder-activated bands [57] arising from random distribution of Ti ions, which can occupy four off-centre sites in the quasi-tetragonal phase. This feature reveals that substrates like CC2 and also the technological process enhance disorder in the ?lms, resulting in a decrease of tetragonality. This spectral property of the BST sensor structure is also visible for the layer deposited on an amorphous glass substrate, as shown in Fig. 4b. However, in this case, the optical Raman shift signal of 634 cm^{-1} is very weak without

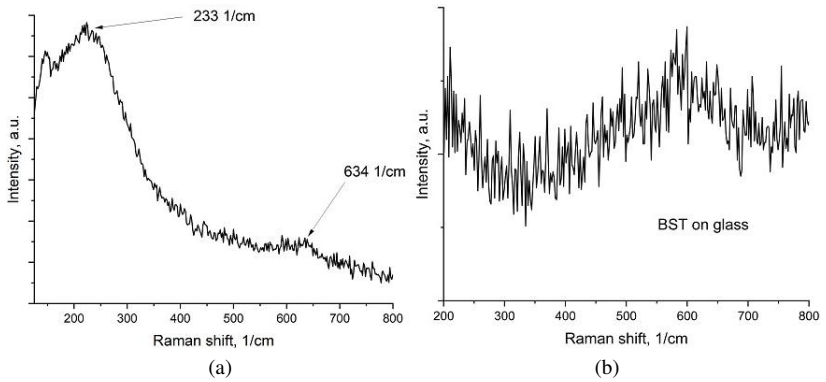

Fig. 4. Raman spectra analysis with BST thin sensing film a) in the range 100 – 800 cm^{-1} – BST signal from electrodes in the area of the CC2 substrate, b) in the range 200 – 800 cm^{-1} – BST deposited on glass substrate.

Metrol. Meas. Syst., Vol. 32 (2025), No. 1, pp. 1–19
DOI: 10.24425/mms.2025.152774

SERS amplification. Utilising Raman spectroscopy for characterization of the sensing layer helps in understanding the underlying chemical and structural changes occurring during sensing processes. This knowledge contributes to the development of more effective, selective and sensitive chemical sensors for a variety of industrial applications.

3.2. Gas-sensing characteristics under NO_2 exposure

The experiments were initially conducted to determine the operating temperature of the sample. As can be observed (Fig. 5a, b), the maximum response was obtained around 205°C +/–2°C. Therefore, further experiments were conducted at different operating temperatures. The calibration curves (0.2–20 ppm of NO_2) in various RH are presented in Fig. 5c, and measurement data is fitted the with $A_1 - A_2 e^{-kx}$ formula with R^2 in the range 0.916–0.956, respectively. The 50% RH level resulted in an enhanced response in the range of concentrations between 0–5 ppm, which is the subject of further analysis.

Within the study, a multi-test was performed to verify the stability of the samples over time. The measurements were made at different operating temperatures (Fig. 5a) and 50% RH. For the NO_2 concentration equal to 5 ppm, a stability test was performed for ten measurement cycles of

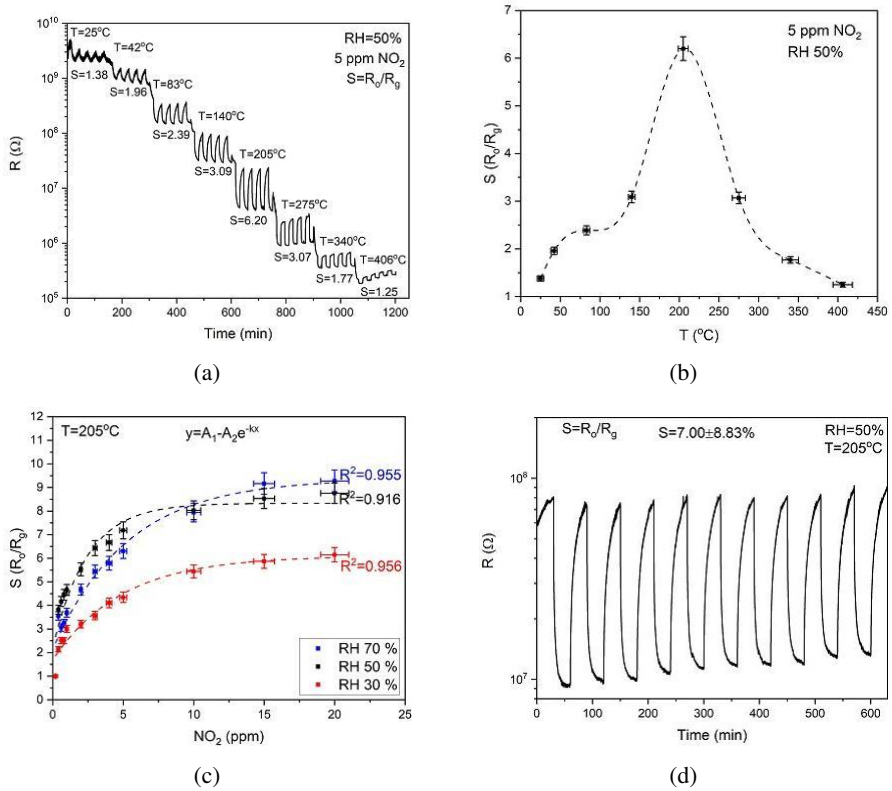

Fig. 5. Sensor test results: (a) sample response to 5 ppm NO_2 at 50% RH as a function of time; (b) sample response to 5 ppm NO_2 at 50% RH as a function of temperature; (c) the response of the sample at operating temperature to various concentrations of NO_2 from 0.2 ppm to 20 ppm at 50% RH; (d) the results of measurements of stability of the sensors.

30 min/30 min (air/air + NO_2) at various temperatures and RH 50%. Figure 6d shows the results of the stable operation tests. Measurements on the sample were conducted for several weeks at different temperatures, RH levels, and NO_2 concentrations; during this time, no change in the sensor properties of the sample was observed.

3.3. Impedance spectroscopy

The impedance spectra in Bode and Nyquist representation (Z" plotted against Z') and fitting results for the prepared sample of BST at the temperatures of 205°C in air and under NO_2 exposure (0.5–5 ppm) across a wide frequency range from 10^{-1} Hz to 10^6 Hz are shown in Figs 6 and 7. The images of the impedance spectra correspond to the obtained results of the gas characteristics of the BST layer under the influence of NO_2 (Fig. 5b). This can be seen at a temperature of 205°C, where the highest sensor response of the sample was S = 6.20 (Fig. 5a).

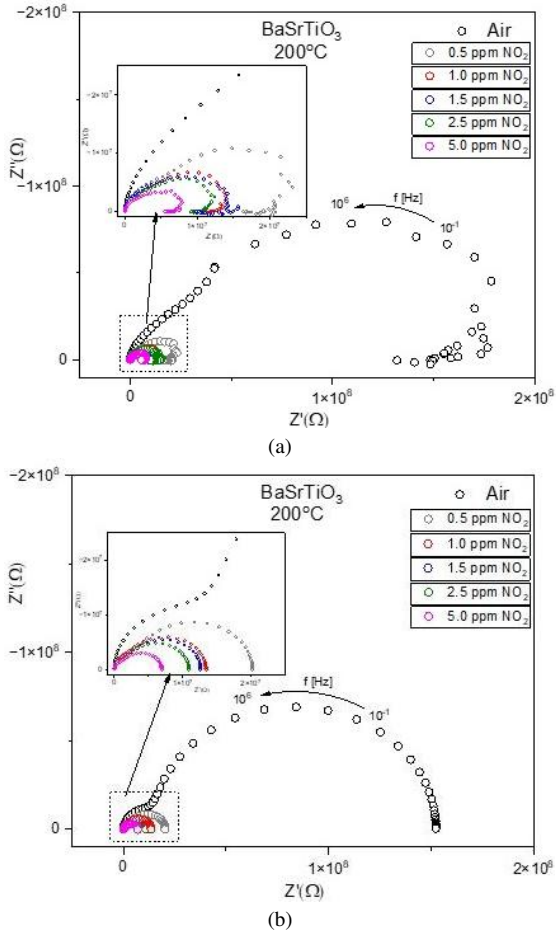

Fig. 6. Impedance spectra of the nanomaterials at an operating temperature of 205°C in air and upon NO_2 exposure (0.5–5 ppm): (a) Nyquist representation $BaSrTiO_3$; (b) fitting – Nyquist representation $BaSrTiO_3$.

Metrol. Meas. Syst., Vol. 32 (2025), No. 1, pp. 1–19
DOI: 10.24425/mms.2025.152774

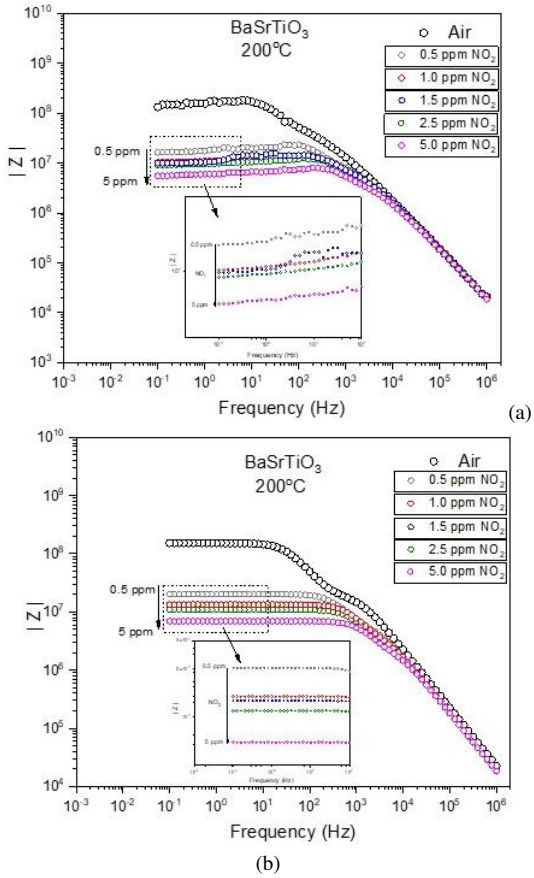

Fig. 7. Impedance spectra of the nanomaterials at an operating temperature of 205°C in air and upon NO_2 exposure (0.5–5 ppm): (a) Bode representation $BaSrTiO_3$; (b) fitting – Bode representation $BaSrTiO_3$.

3.4. Modelling the equivalent circuit

Basic electrical circuits are employed to produce synthetic impedance graphs that depict the experimental data. These circuits may comprise resistors, capacitors, inductors or non-ideal components like *constant phase elements* (CPE). Once the impedance characteristics are plotted, comparisons can be made with typical or established equivalent electrical circuits, leading to an initial comparison with the experimentally measured impedance. Understanding the occurring physicochemical processes and maximising the simplification of the obtained results is a prerequisite for accurate use of circuit modelling. In the analysis of experimental data, one can usually encounter many equivalent circuits that numerically match the obtained results. However, only one of them can provide a realistic picture of electrical characteristics of the sample. Two types of models were proposed for the obtained results (Fig. 8).

Figure 9 presents a graphical representation of the obtained parameters of the equivalent circuit models (R1, R2, C1, C2).

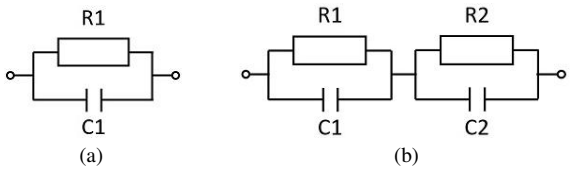

Fig. 8. Proposition of equivalent circuit models: a) model for operating temperature of 205°C upon NO_2 exposure (1.5, 2 and 5 ppm) and 350°C upon NO_2 exposure (2.5 ppm); b) model for the other of operating temperatures and NO_2 exposures.

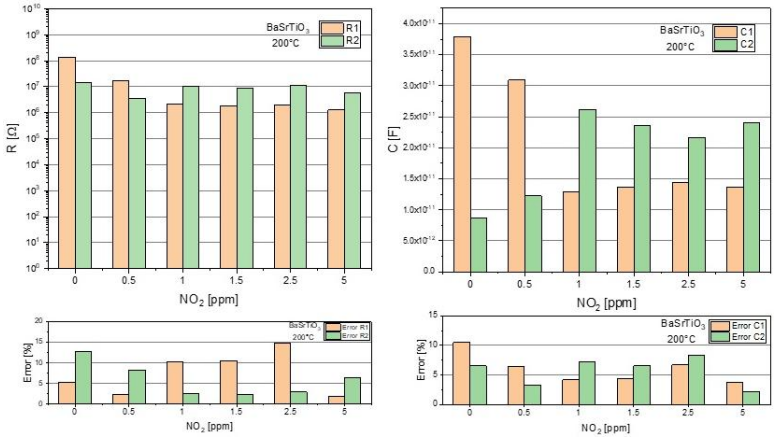

Fig. 9. Graphical representation of the obtained parameters of the equivalent circuit model (R1, R2, C1, C2) at an operating temperature of 205°C in air and upon NO_2 exposure (0.5–5 ppm) and error columns [%].

4. Discussion

The use of impedance spectroscopy to study electrical properties of materials and systems allows for a direct comparison of behaviour of a real object with its substitute system, known as an equivalent model. The substitute impedance system always refers to a physically realized impedance. The analysis and fitting of experimental data to the response of the mathematical model are based on the least squares method. Simulation and fitting are most commonly performed using computer programs developed by Macdonald and Boukamp. However, there is a risk that the developed model may not accurately reproduce reality. This is because the measured characteristics can often be described by different equivalent systems, while only the simplest of them represent specific physical processes.

Approximating the impedance of a physical object using an equivalent model, regardless of the measurement method, allows for verification of the accuracy of the model by comparing characteristics in a specified frequency range. In AC measurements, real and imaginary components of impedance or admittance of the measured object are usually obtained. It should be assumed that the measurement provides information about the components of impedance or admittance. The proper selection of the equivalent model is also important, which should not only approximate the measured characteristics but also physically describe the phenomena occurring in the tested object [58].

In the presence of gas, at selected temperatures (*e.g.* at 205°C (Fig. 6)), characteristics appear in the shape of two interconnected semi-circles. However, the ratio of these two semi-circles is not as equal as is found with other temperatures. This may be due to the different time constants of these circuits. Moreover, some of that data has shoulders at around 10^3 to 10^4 Hz. The shoulders

Metrol. Meas. Syst., Vol. 32 (2025), No. 1, pp. 1–19
DOI: 10.24425/mms.2025.152774

around the frequencies around 10^3 Hz and 10^4 Hz result from the selected model of parallelly connected R and C elements with different values. One semicircle flows smoothly into the other, which results from their separate time constants. This is also visible on the Nyquist and Bode representation of $BaSrTiO_3$ in Figure 10.

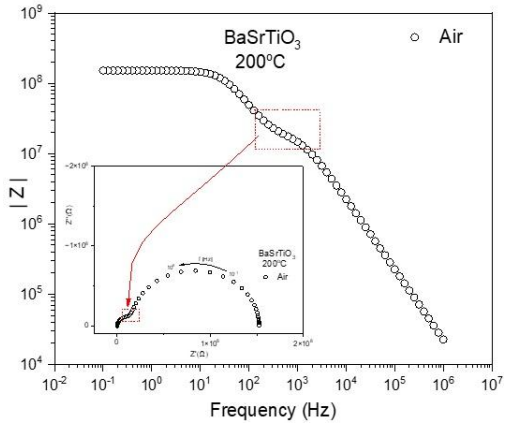

Fig. 10. Impedance spectra of the nanomaterials at an operating temperature of 205°C in air – fitting Nyquist and Bode representation of $BaSrTiO_3$.

Similar experiments were considered in work [14], where various equivalent circuits, including circuits with RC elements, were analysed and interpreted using impedance spectroscopy for semiconductor oxide-based gas sensors.

The Debye response is a key element of impedance spectroscopy characterised by a single time constant denoted "τ". This response consists of a parallel capacitance C with a combination of resistor R. The resistance R models dissipation effects. The capacitor C represents the stored charge. Finally, the relaxation time or time constant can be determined by the equation $\tau = RC$ [10]. When a substrate is present, it is desirable to separate its capacitance from the measurements to focus on the response of the oxide particles. This is especially important when dealing with thin films and nanowire devices for which the capacitance can be very small compared to the substrate [23]. In addition, relaxation frequencies depend only on the intrinsic properties of the material and not on the sample geometrical factors [3] (Tab. 1).

Table 1. Time constant $\tau = RC$ and relaxation frequencies f_R at an operating temperature of 205°C in air and upon NO_2 exposure (0.5–5 ppm).

Temperature 205°C												
	Air		NO_2 – 0.5 [ppm]		NO_2 – 1 [ppm]		NO_2 – 1.5 [ppm]		NO_2 – 2.5 [ppm]		NO_2 – 5 [ppm]	
Element	Value [s]	f_R [Hz]	Value [s]	f_R [Hz]	Value [s]	f_R [Hz]	Value [s]	f_R [Hz]	Value [s]	f_R [Hz]	Value [s]	f_R [Hz]
R1 [Ω]	5.19 E-03	3.07 E+01	5.17 E-04	3.08 E+02	2.86 E-05	5.56 E+03	2.51 E-05	6.35 E+03	2.92 E-05	5.45 E+03	1.73 E-05	9.18 E+03
C1[F]												
R2 [Ω]	1.29 E-04	1.24 E+03	4.40 E-05	3.62 E+03	2.72 E-04	5.85 E+02	2.14 E-04	7.43 E+03	2.46 E-04	6.47 E+02	1.36 E-04	1.17 E+03
C2 [F]												

At higher temperatures, the participation of processes occurring at high frequencies can be seen. This is due to the processes occurring in the inter-grain region and in the bulk. The characterisation of various regions of a sample according to their electrical relaxation times and time constants can be achieved by examining a range of frequencies (10^{-1} Hz to 10^6 Hz). In certain situations, the overall impedance of electrically inhomogeneous materials may be dominated by the resistance at the grain boundary, indicating that these materials are not uniform in their electrical properties. Based on our findings and the impedance spectrum analysis of the equivalent circuit, we hypothesised that the elements C1 and R1 correspond to the capacitance and resistance of the grain bulk, respectively, while C2 and R2 correspond to the capacitance and resistance of the BST grain boundaries.

5. Conclusions

The acquired BST-based gas-sensing layers demonstrated the highest responses at around 205°C and exhibited satisfactory performance within the 0.5–20 ppm range. Nevertheless, beyond 10 ppm, the sensor response plateaued (as illustrated in Fig. 5c). The paper presents the results that are the basis for stating that the obtained BST layer is gas-sensitive to the presence of gaseous NO_2. In addition, an attempt was made to create a broadband impedance model, which was analysed and discussed. The impedance analysis showed that the selected broadband models consisting of single and parallel RC elements in all analysed cases reflect the mechanism of NO_2 gas interaction on the tested gas-sensitive layer of the BST material by changing the parameters. The model is characterised by a fitting error of a few percent at 100°C, 205°C and 300°C.The exception is the high temperature of 350°C, where discrepancies between the actual and reference values begin to be visible. This is caused by, among other factors, the loss of properties of the obtained layer at temperatures above 350°C, and consequently by its degradation and destruction. The data collected from the measurements enables the identification of the most effective working parameters of impedance sensors, including the optimal temperature, frequency, and amplitude of the measurement signal. This information can be utilised in the design of a sensor structure comprising a ceramic substrate, heater, gas-sensitive layer, electrodes and wires, thereby improving the sensitivity and selectivity of the sensors. The direction of further research is to create a sensor and model that will be characterised by such features as high 3S: sensitivity, selectivity and stability. Additionally, the sensor's response was observed to be highly consistent (Fig. 5d), indicating the potential for the use of BST of NO_2 gas sensors in industrial settings.

Acknowledgements

The work was financially supported by the National Science Centre Poland under grant NCN OPUS 2021/41/B/ST7/00276.

References

[1] Barsoukov, E., & Macdonald, J.R. (Red.). (2005). *Impedance Spectroscopy: Theory, Experiment, and Applications* (1. wyd.). Wiley. https://doi.org/10.1002/0471716243

[2] Boukamp, B.A. (2004). Electrochemical impedance spectroscopy in solid state ionics: Recent advances. *Solid State Ionics*, *169*(1–4), 65–73. https://doi.org/10.1016/j.ssi.2003.07.002

Metrol. Meas. Syst., Vol. 32 (2025), No. 1, pp. 1–19
DOI: 10.24425/mms.2025.152774

[3] Irvine, J.T.S., Sinclair, D.C., & West, A.R. (1990). Electroceramics: Characterization by Impedance Spectroscopy. *Advanced Materials*, *2*(3), 132–138. https://doi.org/10.1002/adma.19900020304

[4] K'Owino, I.O., & Sadik, O.A. (2005). Impedance spectroscopy: A powerful tool for rapid biomolecular screening and cell culture monitoring. *Electroanalysis: An International Journal Devoted to Fundamental and Practical Aspects of Electroanalysis*, *17*(23), 2101–2113. https://doi.org/10.1002/elan.200503371

[5] Dean, D., Ramanathan, T., Machado, D., & Sundararajan, R. (2008). Electrical impedance spectroscopy study of biological tissues. *Journal of Electrostatics*, *66*(3–4), 165–177. https://doi.org/10.1016/j.elstat.2007.11.005

[6] Randviir, E.P., & Banks, C.E. (2013). Electrochemical impedance spectroscopy: An overview of bioanalytical applications. *Analytical Methods*, *5*(5), 1098. https://doi.org/10.1039/c3ay26476a

[7] Park, S.-M., & Yoo, J.-S. (2003). Peer reviewed: Electrochemical impedance spectroscopy for better electrochemical measurements. *Analytical Chemistry, Vol 75, Issue 21, 455 A–461 A*. https://doi.org/10.1021/ac0313973

[8] Ciucci, F. (2019). Modeling electrochemical impedance spectroscopy. *Current Opinion in Electrochemistry*, *13*, 132–139. https://doi.org/10.1016/j.coelec.2018.12.003

[9] Wang, S., Zhang, J., Gharbi, O., Vivier, V., Gao, M., & Orazem, M.E. (2021). Electrochemical impedance spectroscopy. *Nature Reviews Methods Primers*, *1*(1), 41. https://doi.org/10.1038/s43586-021-00039-w

[10] Macdonald, J. (2005). Impedance spectroscopy: Models, data fitting, and analysis. *Solid State Ionics*, *176*(25–28), 1961–1969. https://doi.org/10.1016/j.ssi.2004.05.035

[11] Balasubramani, V. (2020). Review — Recent Advances in Electrochemical Impedance Spectroscopy Based Toxic Gas Sensors Using Semiconducting Metal Oxides. *Journal of the Electrochemical Society*. https://doi.org/10.1149/1945-7111/ab77a0

[12] Labidi, A., Jacolin, C., Bendahan, M., Abdelghani, A., Guerin, J., Aguir, K., & Maaref, M. (2005). Impedance spectroscopy on WO_3 gas sensor. *Sensors and Actuators B: Chemical*, *106*(2), 713–718. https://doi.org/10.1016/j.snb.2004.09.022

[13] Paleczek, A., Szafraniak, B., Fuśnik, Ł., Brudnik, A., Grochala, D., Kluska, S., Jurzecka-Szymacha, M., Maciak, E., Kałużyński, P., & Rydosz, A. (2021). The Heterostructures of CuO and SnO_x for NO_2 Detection. *Sensors*, *21*(13), 4387. https://doi.org/10.3390/s21134387

[14] Schipani, F., Miller, D.R., Ponce, M.A., Aldao, C.M., Akbar, S.A., & Morris, P.A. (2016). Electrical Characterization of Semiconductor Oxide-Based Gas Sensors Using Impedance Spectroscopy: A Review. *Reviews in Advanced Sciences and Engineering*, *5*(1), 86–105. https://doi.org/10.1166/rase.2016.1109

[15] Szafraniak, B., Kusior, A., Radecka, M., & Zakrzewska, K. (2020). Impedance spectroscopy in H_2 sensing with TiO_2/SnO_2 nanomaterials. *Metrology and Measurement Systems*, *27*(3), 417–425. https://doi.org/10.24425/mms.2020.134588

[16] Macdonald, D.D. (1990). Some advantages and pitfalls of electrochemical impedance spectroscopy. *Corrosion*, *46*(3), 229–242.

[17] Schipani, F., Miller, D.R., Ponce, M.A., Aldao, C.M., Akbar, S.A., Morris, P.A., & Xu, J.C. (2017). Conduction mechanisms in SnO_2 single-nanowire gas sensors: An impedance spectroscopy study. *Sensors and Actuators B: Chemical*, *241*, 99–108. https://doi.org/10.1016/j.snb.2016.10.061

[18] European Environment Agency. & European Topic Centre on Air Pollution and Climate Change Mitigation (ETC/ACM). (2018). *Air quality in Europe: 2018 report.* Publications Office. https://doi.org/10.2800/777411

[19] World Health Organization. Regional Office for Europe. (2013). *Health effects of particulate matter: Policy implications for countries in Eastern Europe, Caucasus and Central Asia*. World Health Organization. Regional Office for Europe; WHO IRIS. https://apps.who.int/iris/handle/10665/344854

[20] Choi, M.S., Na, H.G., Mirzaei, A., Bang, J.H., Oum, W., Han, S., Choi, S.-W., Kim, M., Jin, C., Kim, S.S., & Kim, H.W. (2019). Room-temperature NO_2 sensor based on electrochemically etched porous silicon. *Journal of Alloys and Compounds*, *811*, 151975. https://doi.org/10.1016/j.jallcom.2019.151975

[21] Akbari, E., Jahanbin, K., Afroozeh, A., Yupapin, P., & Buntat, Z. (2018). Brief review of monolayer molybdenum disulfide application in gas sensor. *Physica B: Condensed Matter*, *545*, 510–518. https://doi.org/10.1016/j.physb.2018.06.033

[22] Rana, Md.M., Ibrahim, D.Sh., Mohd Asyraf, M.R., Jarin, S., & Tomal, A. (2017). A review on recent advances of CNTs as gas sensors. *Sensor Review*, *37*(2), 127–136. https://doi.org/10.1108/SR-10-2016-0230

[23] Toda, K., Furue, R., & Hayami, S. (2015). Recent progress in applications of graphene oxide for gas sensing: A review. *Analytica Chimica Acta*, *878*, 43–53. https://doi.org/10.1016/j.aca.2015.02.002

[24] Zhang, C., Luo, Y., Xu, J., & Debliquy, M. (2019). Room temperature conductive type metal oxide semiconductor gas sensors for NO_2 detection. *Sensors and Actuators A: Physical*, *289*, 118–133. https://doi.org/10.1016/j.sna.2019.02.027

[25] Simon, I., Bârsan, N., Bauer, M., & Weimar, U. (2001). Micromachined metal oxide gas sensors: Opportunities to improve sensor performance. *Sensors and Actuators B: Chemical*, *73*(1), 1–26. https://doi.org/10.1016/S0925-4005(00)00639-0

[26] Staerz, A., Weimar, U., & Barsan, N. (2022). Current state of knowledge on the metal oxide based gas sensing mechanism. *Sensors and Actuators B: Chemical*, *358*, 131531. https://doi.org/10.1016/j.snb.2022.131531

[27] Aleixandre, M., & Gerboles, M. (2012). Review of small commercial sensors for indicative monitoring of ambient gas. *Chem. Eng. Trans*, *30*. https://doi.org/10.3303/CET1230029

[28] Szafraniak, B., Fuśnik, Ł., Xu, J., Gao, F., Brudnik, A., & Rydosz, A. (2021). Semiconducting Metal Oxides: $SrTiO_3$, $BaTiO_3$ and $BaSrTiO_3$ in Gas-Sensing Applications: A Review. *Coatings*, *11*(2), 185. https://doi.org/10.3390/coatings11020185

[29] Xu, J., Liu, S., Wang, Y., Guo, Y., Zhao, J., Yan, H., & Gao, F. (2020). Enhanced dielectric properties of highly dense $Ba_{0.5}Sr_{0.5}TiO_3$ ceramics via non-toxic gelcasting. *Journal of Materials Science: Materials in Electronics*, *31*(20), 17819–17827. https://doi.org/10.1007/s10854-020-04336-0

[30] Liu, Y., Nagra, A.S., Erker, E.G., Periaswamy, P., Taylor, T.R., Speck, J., & York, R.A. (2000). $BaSrTiO_3$ Interdigitated Capacitors for Distributed Phase Shifter Applications. *IEEE Microwave and Guided Wave Letters*, *10*(11). https://doi.org/10.1109/75.888828

[31] Shen, Z.-Y., Wang, Y., Tang, Y., Yu, Y., Luo, W.-Q., Wang, X., Li, Y., Wang, Z., & Song, F. (2019). Glass modified barium strontium titanate ceramics for energy storage capacitor at elevated temperatures. *Journal of Materiomics*, *5*(4), 641–648. https://doi.org/10.1016/j.jmat.2019.06.003

[32] Borderon, C., Nadaud, K., Coulibaly, M., Renoud, R., & Gundel, H. (2019). Mn-Doped $Ba_{0.8}$ $Sr_{0.2}TiO_3$ Thin Films for Energy Storage Capacitors. *International Journal of Advanced Research in Physical Science*, *6*(2), 2349–7882.

[33] Roy, S.C. (2004). *Electrical optical and gas sensing properties of $Ba_xSr_{1-x}TiO_3$ thin films prepared by sol-gel process*. [Doctoral dissertation, Indian Institute of Technology Delhi].

Metrol. Meas. Syst., Vol. 32 (2025), No. 1, pp. 1–19
DOI: 10.24425/mms.2025.152774

[34] Stanoiu, A., Piticescu, R.M., Simion, C.E., Rusti-Ciobota, C.F., Florea, O.G., Teodorescu, V.S., Osiceanu, P., Sobetkii, A., & Badilita, V. (2018). H_2S selective sensitivity of Cu doped $BaSrTiO_3$ under operando conditions and the associated sensing mechanism. *Sensors and Actuators B: Chemical*, *264*, 327–336. https://doi.org/10.1016/j.snb.2018.03.013

[35] Roy, S.C., Sharma, G.L., Bhatnagar, M.C., & Samanta, S.B. (2005). Novel ammonia-sensing phenomena in sol–gel derived $Ba_{0.5}Sr_{0.5}TiO_3$ thin films. *Sensors and Actuators B: Chemical*, *110*(2), 299–303. https://doi.org/10.1016/j.snb.2005.02.030

[36] Patil, R.P., Gaikwad, S.S., Karanjekar, A.N., Khanna, P.K., Jain, G.H., Gaikwad, V.B., More, P.V., & Bisht, N. (2020). Optimization of strontium-doping concentration in $BaTiO_3$ nanostructures for room temperature NH_3 and NO_2 gas sensing. *Materials Today Chemistry*, *16*, 100240. https://doi.org/10.1016/j.mtchem.2019.100240

[37] Sharma, S., Sharma, A., Tomar, M., Puri, N.K., & Gupta, V. (2014). NOx Sensing Properties of Barium Titanate Thin Films. *Procedia Engineering*, *87*, 1067–1070. https://doi.org/10.1016/j.proeng.2014.11.347

[38] BVT Technologie. (2024, September 9). *CC2 Electrochemical sensor*. https://bvt.cz/produkt/cc2/

[39] Rydosz, A., & Szkudlarek, A. (2015). Gas-sensing performance of M-doped CuO-based thin films working at different temperatures upon exposure to propane. *Sensors*, *15*(8), 20069–20085. https://doi.org/10.3390/s150820069

[40] Liu, S., Guo, Y., Li, J., Wu, S., Xu, J., Pawlikowska, E., Kong, J., Rydosz, A.M., Szafran, M., & Gao, F. (2022). Microstructure and dielectric properties of $(Ba_{0.6}Sr_{0.4})TiO_3$/PEEK functional composites prepared via cold-pressing sintering. *Composites Science and Technology*, *219*, 109228. https://doi.org/10.1016/j.compscitech.2021.109228

[41] Guo, Y., Liu, S., Wu, S., Xu, J., Pawlikowska, E., Bulejak, W., Szafran, M., Rydosz, A., & Gao, F. (2022). Enhanced tunable dielectric properties of $Ba_{0.6}Sr_{0.4}TiO_3$/PVDF composites through dual-gradient structural engineering. *Journal of Alloys and Compounds*, *920*, 166034. https://doi.org/10.1016/j.jallcom.2022.166034

[42] Guo, Y., Wu, S., Liu, S., Xu, J., Pawlikowska, E., Szafran, M., Rydosz, A., & Gao, F. (2022). Enhanced dielectric tunability and energy storage density of sandwich-structured $Ba_{0.6}Sr_{0.4}TiO_3$/PVDF composites. *Materials Letters*, *306*, 130910. https://doi.org/10.1016/j.matlet.2021.130910

[43] Grundström, M., Hak, C., Chen, D., Hallquist, M., & Pleijel, H. (2015). Variation and co-variation of PM10, particle number concentration, NO_x and NO_2 in the urban air – Relationships with wind speed, vertical temperature gradient and weather type. *Atmospheric Environment*, *120*, 317–327. https://doi.org/10.1016/j.atmosenv.2015.08.057

[44] Tsiulyanu, D., Marian, S., Liess, H.-D., & Eisele, I. (2004). Effect of annealing and temperature on the NO_2 sensing properties of tellurium based films. *Sensors and Actuators B: Chemical*, *100*(3), 380–386. https://doi.org/10.1016/j.snb.2004.02.005

[45] Chai, H., Zheng, Z., Liu, K., Xu, J., Wu, K., Luo, Y., Liao, H., Debliquy, M., & Zhang, C. (2022). Stability of Metal Oxide Semiconductor Gas Sensors: A Review. *IEEE Sensors Journal*, *22*(6), 5470–5481. https://doi.org/10.1109/JSEN.2022.3148264

[46] Eranna, G., Joshi, B., Runthala, D., & Gupta, R. (2004). Oxide materials for development of integrated gas sensors — A comprehensive review. *Critical Reviews in Solid State and Materials Sciences*, *29*(3–4), 111–188.

[47] Wei, P., Ning, Z., Ye, S., Sun, L., Yang, F., Wong, K.C., Westerdahl, D., & Louie, P.K. (2018). Impact analysis of temperature and humidity conditions on electrochemical sensor response in ambient air quality monitoring. *Sensors*, *18*(2), 59.

[48] Maier, K., Helwig, A., Müller, G., Hille, P., & Eickhoff, M. (2015). Effect of Water Vapor and Surface Morphology on the Low Temperature Response of Metal Oxide Semiconductor Gas Sensors. *Materials*, *8*(9), 6570–6588. https://doi.org/10.3390/ma8095323

[49] Raju, P., & Li, Q. (2022). Review — Semiconductor Materials and Devices for Gas Sensors. *Journal of the Electrochemical Society*, *169*(5), 057518. https://doi.org/10.1149/1945-7111/ac6e0a

[50] Herrmann, J.-M., Disdier, J., Fernandez, A., Jimenez, V., & Sanchez-Lopez, J. (1997). Oxygen gas sensing behavior of nanocrystalline tin oxide prepared by the gas phase condensation method. *Nanostructured Materials*, *8*(6), 675–686. https://doi.org/10.1016/S0965-9773(97)00224-9

[51] Ghosh, A., Late, D.J., Panchakarla, L.S., Govindaraj, A., & Rao, C.N.R. (2009). NO_2 and humidity sensing characteristics of few-layer graphenes. *Journal of Experimental Nanoscience*, *4*(4), 313–322. https://doi.org/10.1080/17458080903115379

[52] Li, Q., Zeng, W., & Li, Y. (2022). Metal oxide gas sensors for detecting NO_2 in industrial exhaust gas: Recent developments. *Sensors and Actuators B: Chemical*, *359*, 131579. https://doi.org/10.1016/j.snb.2022.131579

[53] Scribner. (2024, September 9). ZView®for Windows. https://www.scribner.com/software/68-general-electrochemistr376-zview-for-windows/

[54] Yuzyuk, Y.I. (2012). Raman scattering spectra of ceramics, films, and superlattices of ferroelectric perovskites: A review. *Physics of the Solid State*, *54*, 1026–1059.

[55] Fang, P., He, M., Xie, Y., & Luo, M. (2006). XRD and Raman spectroscopic comparative study on phase transformation of gamma-Al_2O_3 at high temperature. *Spectroscopy and Spectral Analysis*, *26*(11), 2039–2042. PMID:17260751

[56] Bulyarskii, S., Kozhevin, A., Mikov, S., & Prikhodko, V. (2000). Anomalous R-line behaviour in nanocrystalline Al_2O_3:Cr_{3+}. *Physica Status Solidi (a)*, *180*(2), 555–560. https://doi.org/10.1002/1521-396X(200008)180:2%3C555:AID-PSSA555%3E3.0.CO;2-D

[57] Yuzyuk, Y.I., Sauvajol, J., Simon, P., Lorman, V., Alyoshin, V., Zakharchenko, I., & Sviridov, E. (2003). Phase transitions in ($Ba_{0.7}$ $Sr_{0.3}$)TiO_3/(001)MgO thin film studied by Raman scattering. *Journal of Applied Physics*, *93*(12), 9930–9937.

[58] Nitsch, K. (1999). *Zastosowanie spektroskopii impedancyjnej w badaniach materiałów elektronicznych*. Oficyna Wydawnicza Politechniki Wrocławskiej.

Bartłomiej Szafraniak received his M..Sc degree in electrical engineering from the AGH University of Science and Technology in Kraków, Poland in 2014. Currently, he is a PhD student at the AGH UST. Since 2019, he has worked as a research and teaching assistant at the Institute of Electronics of the Faculty of Computer Science, Electronics, and Telecommunications of the same university. His main research focuses on the use of impedance spectroscopy to analyse the response of tested materials and an attempt to create their appropriate equivalent electrical model.

Sabina Drewniak received the Ph.D. degree from the Silesian University of Technology, Poland, in 2016. She has co-authored 33 journal papers. Her research activity focuses on gas sensing materials, in particular graphene and reduced graphene oxide. She is also interested in characterization of sensor's materials using, among others, Raman spectroscopy, FTIR spectroscopy, and various kinds of surface imaging.

Metrol. Meas. Syst., Vol. 32 (2025), No. 1, pp. 1–19
DOI: 10.24425/mms.2025.152774

Łukasz Fuśnik he received his M.Sc. degree in Power Engineering from the AGH University of Science and Technology in Cracow, Poland In 2012. Between 2012 and 2016, he was working in the Electrical Energy Distribution Department of PKP Energetyka S.A. Between as well as in the Department of Electrical and Power Engineering AGH UST. Since 2019 he has been working in the Department of Electronics AGH UST. Since 2014 he has been a PhD student at the AGH UST. His main research focuses on determination of wideband characteristics of power transformer's windings.

Artur Rydosz received his MSc and PhD in electronics engineering from the AGH University of Science and Technology, Krakow, Poland in 2009 and 2014, respectively. His scientific interests focus on the PVD method of fabricating various sensing materials with special emphasis on the detection of volatile organic compounds in exhaled human breath, for example, as a potential tool for noninvasive measurements of several diseases, such as diabetes. Since 2019, he has worked as a professor at the Department of Electronics AGH and serves as the Vice-chair of the Joint Chapter AP03/AES10/MTT17, IEEE Poland Section. He was awarded several awards for young researchers, including START 2015, and START 2016 from the Foundation for Polish Science, Ministry of Science and Higher Education, and recently from the POLITYKA journal. He is a member of several societies, such as the Polish Vacuum Society, the Polish Sensor Society, the IMAPS, the 500 Innovators Society, the Section of Microwaves and Radiolocation, Polish Academy of Science.

Jie Xu is currently an Associate Professor at the School of Materials Science and Engineering at Northwestern Polytechnical University. He received a Ph.D. degree from the School of Materials Science and Engineering at Tsinghua University, Beijing, China, in 2004. His research interests are the development of porous ceramics, high-entropy ceramics, and thermal insulating materials.

Feng Gao is currently a Full Professor at the School of Materials Science and Engineering of Northwestern Polytechnical University (NPU), Director of the Department of Materials Science and Engineering at NPU, Chief-scientist of QMUL-NPU Joint Research Institute of Advanced Materials and Structures (AMAS), and a Senior Member of the Chinese Materials Research Society. He received degrees of B.E., M.E. and Ph.D. in Materials Science and Engineering from NPU in Xi'an from 1992 to 2002. Following postdoctoral work at the Postdoctoral Mobile Station of Aerospace Science and Technology in NPU from 2003 to 2005, he worked at the Pennsylvania State University, USA, as a visiting scholar. His main research interests are development of advanced functional ceramics such as ferroelectric, piezoelectric, thermoelectric, microwave dielectric ceramics, *etc.* and devices. He has co-authored more than 200 papers in professional journals.

Andrzej Brudnik obtained the Ph.D. in electronics in 1997 and hishis habilitation in the same field in 2014. His research activity focuses on thin films technology, with particular emphasis on the diagnostics of the reactive magnetron sputtering process. He is currently a Professor with the Institute of Electronic – AGH University, Krakow, Poland.

Łukasz Błajszczak obtain the B. Eng. (2020) and M. Sc. (2021) degree in mechanical engineerig and he is currently a Ph. D. student in materials engineering at AGH University of Krakow. His research activity focuses on laser surface modification, electrochemical spectroscopy impedance and SEM investigations with EDS analysis.

Erwin Maciak received the Ph.D. degree from the Silesian University of Technology, in 2005. He is currently an Associate Professor and the Head of Department of Optoelectronics at the same university. He has authored or coauthored over 60 scientific papers (Scopus) and he holds 7 issued Polish patents. His main current research interests include developing chemo-optical and chemo-electronic sensor structures for optoelectronic and microelectronic gas sensors for applications in the detection of chemical analytes. EHe has expertise in conducting research and interpreting measurement results obtained through methods used, among others, for nanoindentation of sensor materials. Additionally, he has had experience in carrying out various interdisciplinary tasks, initiatives, research projects, and educational projects in collaboration with national and international academic institutions and business entities.